Antialiasing and wave equation statics by series approximation and inversion

Robert J. Ferguson

ABSTRACT

To address the problems of irregular trace spacing and statics correction, simultaneous regularization and wave equation statics (WE statics) is implemented by least-squares inversion. In general, inversion is found to be intractable currently in 3D, so series approximation is made to reduce significantly the number of required integrals. The resulting operator is suitable for both direct inversion, or for use with gradient methods.

Real and synthetic data are used to demonstrate the viability of the inversion. Synthetic data show that even for severe velocity variation and topography, inversion converges to an acceptable solution, and that aliasing is significantly reduced. Similarly for real data, inversion is shown to return a regularized result with WE statics applied that is anti-aliased.

INTRODUCTION

An inversion for seismic data is given in Ferguson (2006) to correct for strong velocity variation in the near-surface simultaneously with trace regularization. The wave equation statics component of that method is implemented with an approach related to the *migration by deconvolution* of Yu et al. (2006) where operator error associated with lateral heterogeneity (Etgen, 1994) is mitigated through least-squares inversion. Ferguson (2006) adds regularization to least-squares inversion to regularize data and reduce operator error for negligible additional cost. The analytic basis for this method results in a multidimensional Fourier integral, and an approximation is developed there to reduce computational effort. That approximation achieves efficiency through computation of only the central diagonals of the associated wavefield operators, so it is an approximation that has no analytical justification. Here, a new analytic basis is provided for approximation through series approximation and truncation. This approach provides an analytic form that is used as a basis for an improved inversion algorithm. This improved algorithm is based on implementation of the Newton method (Tarantola, 1987, pg. 251, for example), but it has direct application to gradient methods (Smith et al., 2009; Tarantola, 1987, pg. 239, for example) where it may be used as a fast approximation to the preconditioning operator.

Central to the method presented here is the use of wave-equation operators to focus irregular wavefields and reduce spatial aliasing. In this way, inversion is similar to regularization methods that require a velocity model. Robertsson et al. (2008), for example, apply a normal-move-out (NMO) correction to data acquired with multicomponent streamer prior to interpolation of crossline pressure measurements. In Güliünay (2003), to help ensure that the dip content of lower frequencies is similar to that of linear events in the input, NMO correction is applied prior to prediction error filtering. In a least-squares inversion that is similar to the approach proposed here, modified Stolt (Stolt, 1978) and Kirchhoff (Schneider, 1978) operators are used by Trad (2003) to localize hyperbolic events and solve a similar equation by gradient methods.

A number of other interpolation / regularization methods are based on the $f - x$ method of Spitz (1991). Naghizadeh and Sacchi (2009) extend $f - x$ interpolation for variable dips using adaptive prediction filters. For regularization, Zwartjes and Sacchi (2007) extend Spitz (1991) through the use of the non-uniform Fourier transform (NFFT) (Duijndam and Schonewille, 1999, for example).

Under the heading of Fourier reconstruction methods, Hennenfent and Herrmann (2008) demonstrate that random undersampling is better than regular undersampling. Abma and Kabir (2006) use an iterative Fourier method to regularize data, and Duijndam et al. (1999) use least-squares to estimate a regularized Fourier spectrum. In their method, Duijndam et al. (1999) use energy-adaptive stabilization and noise adaptive weighting in a stable and efficient regularization.

In this paper, a number of ideas from the above authors are adapted to the problem of trace regularization and wave-equation statics application. Similar to Trad (2003), for example, wave-equation operators are used to localize reflection energy, and weighting operators are used to ensure stability and minimize noise. Here, rather than Stolt and Kirchhoff operators, one-way operators are used to ensure accuracy and multipathing in heterogeneous media.

From the general expression for regularization and redatum by the Newton method (Ferguson, 2006), I depart from this development at the point of approximation of the Hessian. Where Ferguson (2006) offers a sparse matrix-operator that is fast to compute, an asymptotic expansion is developed here and then truncated. This results in significant computational savings, and it makes this inversion tractable in 3D.

This approximate inversion is then tested on synthetic data and real data. As a bench mark, inversion (hereafter in this paper, *inversion* will represent the regularization / redatum method presented here) of *irregular*, aliased data is compared to interpolation of *regular*, aliased data that is interpolated using the $f - x$ method [*] of Spitz (1991) followed by WE statics. Equivalent results are found for this benchmark are found. Increasingly irregular synthetic data reveal that, even in the presence of severe variation in velocity and topography, and where data are extremely irregular and aliased, inversion restores missing traces and removes traveltime effects. The real-data example shows similar results even in the presence of strong topography, strong velocity variation, and severe trace decimation.

THEORY

Given monochromatic wavefield ψ_z at depth z, the Newton-method solution for extrapolated wavefield $\psi_{z+\Delta z}$ is

$$\psi_{z+\Delta z} = \left[U^A_{-\Delta z} W_e U_{-\Delta z} + \varepsilon^2 W_m \right]^{-1} U^A_{-\Delta z} W_e \psi_z, \qquad (1)$$

where W_e and W_m are a weighting operator and a minimum-length operator respectively, and ε^2 is a scalar that controls the amount of smoothing (Ferguson, 2006; Menke, 1989,

---

[*]Though multi-dimensional regularization methods that outperform $f - x$ interpolation exist (Zwartjes and Sacchi, 2007, for example), they are not as widely available.

pg. 53 - 54). It is assumed in equation 1 that input wavefield ψ_z is an irregularly sampled wavefield that has been infilled with null traces in a prior processing-step. Prior infill gives a wavefield that is regularly sampled, but one with significant error due to the null traces. So that null traces don't influence the solution, diagonal operator W_e weights live traces and null traces, respectively, with unit value and zero value (Menke, 1989, pg. 54). Minimum-length operator W_m ensures that the minimum-length solution is found (Menke, 1989, pg. 53 - 54). Operator $U_{-\Delta z}$ and its adjoint $U^A_{-\Delta z}$ are known as one-way operators that move wavefields distance $-\Delta z$ and $+\Delta z$ along the depth axis respectively according to a user-defined model of seismic velocity (Margrave and Ferguson, 1999).

Computationally, $U_{-\Delta z}$ and $U^A_{-\Delta z}$ are matrices that can be very large; for 2D data, they may have hundreds or thousands of columns and a similar number of rows. In 3D, computation of $\left[U^A_{-\Delta z} W_e U_{-\Delta z} \psi_z \left(x'\right)\right] (x)$ within equation 1 is impossible (practically speaking) in 3D currently.

Ferguson (2006) and Kühl and Sacchi (2004) explore different approximations to

$$S = U^A_{-\Delta z} W_e U_{-\Delta z}, \tag{2}$$

for use within Hessian of equation 1. Kühl and Sacchi (2004) use phaseshift-plus-interpolation (PSPI) (Gazdag and Sguazzero, 1984) within a conjugate gradient framework, and Ferguson (2006) computes and applies directly only a limited number of diagonals for S, and then computes the inverse using an efficient LU operator. This latter inversion results in a dip-limited operator related to $\omega - x$ migration (Berkhout, 1985).

Operator S transforms from space coordinates x' to wavenumber coordinates, and it applies a nonstationary phase shift – operator $U_{-\Delta z}$ does this. The result is then reversed by $U^A_{-\Delta z}$ and transformed back to space coordinates x. Once computed, S is added to minimum-length operator $\varepsilon^2 \mathbf{W_m}$, and the result is inverted. The redatum aspect of the inversion is actually implemented in equation 1 by $U^A_{-\Delta z}$ applied to $W_e \psi_z$ (the weighted input). Extrapolators $U^A_{-\Delta z}$ and $U_{-\Delta z}$ in S act together as a migration-deconvolution operator similar to that of Hu et al. (2001).

For arbitrary wavefield ψ_z, the action of S can be written as a nonstationary convolution (Margrave, 1998)

$$\left[S\psi_z \left(x'\right)\right] (x) = \int \psi_z \left(x'\right) S \left(x, x - x'\right) dx', \tag{3}$$

where x and x' are 2D space coordinates of output and input at recording surface z respectively, and

$$S \left(x, x - x'\right) = \frac{1}{(2\pi)^4} \int e^{-i[k_x, y - x']} e^{-i[k'_x, x - y]} \alpha \left(y, k'_x\right)_{\Delta z} \tilde{\alpha} \left(y, k_x\right)_{-\Delta z} dk_x \, dy \, dk'_x. \tag{4}$$

Two dimensional space coordinate y corresponds to datum $z + \Delta z$, and wavenumbers k_x, and k'_x are wavenumber duals of x and x' respectively. Extrapolator α is

$$\alpha_{\pm \Delta z} = e^{\pm i \Delta z k_z}, \tag{5}$$

and for temporal frequency $|\omega| = \omega$, wavenumbers k_z are

$$k_z = \Re \left\{ k \sqrt{1 - \left(\frac{k_x}{k} \right)^2} \right\} + i \operatorname{sgn}(\Delta z) \left| \Im \left\{ k \sqrt{1 - \left(\frac{k_x}{k} \right)^2} \right\} \right|, \qquad (6)$$

where $k = \frac{\omega}{v}$, and v is seismic velocity that varies laterally with y. This prescription for k_z ensures exponential decay in the evanescent region ($k_z = \Im\{k_z\}$). Extrapolator $\tilde{\alpha}_{-\Delta z}$ results from the application of diagonal weighting operator W_e to $\alpha_{-\Delta z}$.

As it is, operator S is extremely costly to apply, and in 2D for example, cost is $\propto N^3$ floating-point operations (flops) where N is the number of traces (Ferguson, 2006). N^3 is the cost of the inner loop of the inversion, and outside of it is a loop over temporal frequency, and then a loop over depth. So, for hundreds of traces, frequencies, and depths, inversion of a single trace gather can run for hours on a single processor. In 3D, cost of the inner loop grows to $\propto N^8$ flops as is shown in Appendix A (we are interested in the order-of-magnitude-cost, so for simplicity, the number of inline and crossline traces are assumed here to be equal to N). For a 1000×1000 receiver array, for example, minimum cost is $\propto 10^{24}$ flops per frequency per depth.

Approximate Hessian

Because inversion is so costly, some kind of approximation must be considered. Begin with equation 4, and introduce coordinates $\xi = k_x' - k_x$, $k_x' = \xi + k_x$, and $d\xi = dk_x'$ to get

$$S(x, x - x') = \frac{1}{(2\pi)^4} \int e^{iy\xi} e^{ix'k_x} e^{-ix[\xi + k_x]} \alpha(y, \xi + k_x)_{\Delta z} \tilde{\alpha}(y, k_x)_{-\Delta z} \, dk_x \, dy \, d\xi. \quad (7)$$

Expand $\alpha(\xi + k_x)_{\Delta z}$ as a Taylor series in k_x according to

$$\alpha(\xi + k_x)_{\Delta z} = \sum_{j=0}^{\infty} \frac{1}{j!} \left[\partial_{k_x}^j \alpha(k_x)_{\Delta z} \right] \xi^j, \qquad (8)$$

and then compute $y \to \xi$ to eliminate an integral in favour of an infinite sum (that we may expect to truncate later) so that

$$S(x, x - x') = \sum_{j=0}^{\infty} \frac{1}{j!} \frac{1}{(2\pi)^4} \int e^{-ik_x[x - x']} e^{-ix\xi} \xi^j H(\xi, k_x)_{j, \Delta z} \, dk_x \, d\xi, \qquad (9)$$

where

$$H(\xi, k_x)_{j, \Delta z} = \int e^{iy\xi} \left[\partial_{k_x}^j \alpha(y, k_x)_{\Delta z} \right] \tilde{\alpha}(y, k_x)_{-\Delta z} \, dy. \qquad (10)$$

Then, because function f and its spectrum F are related through

$$i^j \partial_x^j f(x) \leftrightarrow \frac{1}{2\pi} \int \xi^j F(\xi) e^{-i\xi x} \, d\xi, \qquad (11)$$

we may compute $\xi \to x$ to eliminate another integral

$$S\left(x, x-x'\right) = \sum_{j=0}^{\infty} \frac{i^j}{j!} \frac{1}{(2\pi)^2} \int e^{-ik_x[x-x']} \left[\partial_x^j h_j\left(x, k_x\right)_{\Delta z}\right] dk_x \qquad (12)$$

where

$$h_j\left(x, k_x\right)_{\Delta z} = \left[\partial_{k_x}^j \alpha\left(x, k_x\right)_{\Delta z}\right] \tilde{\alpha}\left(x, k_x\right)_{-\Delta z}. \qquad (13)$$

Our arrival at equation 12 involves elimination of two integrals (four integrals in 3D) in exchange for the cost associated with differential operators and an infinite sum. For practical implementation, truncate series equation 12 to $n << \infty$ terms so that

$$S\left(x, x-x'\right) \sim \sum_{j=0}^{n} \frac{i^j}{j!} \frac{1}{(2\pi)^2} \int e^{-ik_x[x-x']} \left[\partial_x^j h_j\left(x, k_x\right)_{\Delta z}\right] dk_x. \qquad (14)$$

The cost of this series is dominated by the sum over k_x and j is $\propto N^2 \times$ the number of terms n in the series or $\propto n N^2$ in 3D and $\propto n N$ in 2D. For $n = 4$ and $N = 1000$, for example, 2D cost is $\propto 10^3$ flops per frequency per depth – a 10^6 fold reduction in cost over exact solution (equation 4). For 3D, cost is $\propto 10^{12}$ flops per frequency per depth – a 10^{12} fold reduction in cost relative to the exact solution (Appendix A).

IMPLEMENTATION

In this section, a basic description of the implementation of the inversion is presented. For simplicity, components of the inversion will be rendered in a notation where bold symbols represent matrices, for example, $\boldsymbol{S}\,\boldsymbol{\psi} \leftrightarrow [S\,\psi\,(x')]\,(x)$. To implement equation 14 we have

$$\boldsymbol{S} \sim \sum_{j=0}^{4} \boldsymbol{S}_j, \qquad (15)$$

where, for example,

$$\boldsymbol{S}_0 = \text{FFT}\left\{\boldsymbol{e} \odot \boldsymbol{h}_0\right\}. \qquad (16)$$

In equation 16, FFT indicates fast Fourier transform over k_x, $\boldsymbol{e} \leftrightarrow e^{-i\,k_x\,x}$, $\odot$ indicates the scalar product of matrices, and, from equation 13,

$$\boldsymbol{h}_0 = \boldsymbol{\alpha}_{\Delta z} \odot \tilde{\boldsymbol{\alpha}}_{-\Delta z}, \qquad (17)$$

where $\boldsymbol{\alpha}_{\Delta z} \leftrightarrow e^{i\,\Delta z\,k_z}$, $\tilde{\boldsymbol{\alpha}}_{-\Delta z} = \boldsymbol{\alpha}_{-\Delta z}\,\boldsymbol{W_e}$ (the weighting operator applied to extrapolator $\alpha_{-\Delta z}$), and k_z is given by equation 6 (now as a function of x rather than y). For these matrices, x varies along columns, and k_x varies along rows. The next term, $j = 1$, in the series equation 15 is

$$\boldsymbol{S}_1 = \text{FFT}\left\{\boldsymbol{e} \odot \left[\boldsymbol{h}_1 \boldsymbol{D}^1\right]\right\}, \qquad (18)$$

where $\boldsymbol{D}^1$ is a finite-difference operator for coordinates x with rows $[\cdots 1\ -1\ \cdots] \div \Delta x$, Δx is trace spacing, and

$$\boldsymbol{h}_1 = \left[\boldsymbol{D}^1\,\boldsymbol{\alpha}_{\Delta z}\right] \odot \tilde{\boldsymbol{\alpha}}_{-\Delta z}. \qquad (19)$$

Terms $\boldsymbol{S}_2$, $\boldsymbol{S}_3$, and $\boldsymbol{S}_4$ in equation 15 are constructed similarly.

As an improvement to the preconditioning operator for gradient methods, we would multiply $\boldsymbol{S}$ by minimum-length operator $\boldsymbol{W_m}$, add ones to the main diagonal, and then compute an approximate inverse of the result (Tarantola, 1987, pg. 251, for example). To implement the Newton method, equation 1, we scale $\boldsymbol{W_m}$ by ε^2, add this to $\boldsymbol{S}$, and then compute the inverse of the result. Extrapolated wavefield $\boldsymbol{\psi}_{z+\Delta z}$ (a vector) is then calculated according to

$$\boldsymbol{\psi}_{z+\Delta z} = \left[\boldsymbol{S} + \varepsilon^2\,\boldsymbol{W_m}\right]^{-1}\,\boldsymbol{U}_{-\Delta z}^A\,\boldsymbol{W_e}\,\boldsymbol{\psi}_z, \qquad (20)$$

where $\boldsymbol{W_m}$ is a finite-difference operator with rows $\left[\cdots\ 1\ -2\ \ 1\ \cdots\right] \div \Delta x^2$. Vector $\boldsymbol{U}_{-\Delta z}^A\,\boldsymbol{W_e}\,\boldsymbol{\psi}_z$ in equation 20 is the result of matrix $\boldsymbol{W_e}$ applied to input vector $\boldsymbol{\psi}_{\Delta z}$. Recall, $\boldsymbol{\psi}_{\Delta z}$ is infilled with null traces in a prior step, so $\boldsymbol{W_e}$ has '1's (live trace) and '0's (null trace) along the main diagonal. The result is then phase-shifted by $\boldsymbol{U}_{-\Delta z}^A$ and the inversion operator is applied. Determination of scalar ε^2 is done by trial and error (Menke, 1989, pg. 52). In the current implementation, inverse $\left[\boldsymbol{S} + \varepsilon^2\,\boldsymbol{W_m}\right]^{-1}$ is found through LU decomposition (Press et al., 1999, pg. 48, for example).

The procedure outlined in this section is general in that it is a solution for one frequency, one x-line wavenumber, and one depth step. For time-domain output, $\boldsymbol{\psi}_{z+\Delta z}$ is computed for all positive frequencies ω of interest, and IFFT $\omega \to t$ is computed. For 3D, equation 20 is applied iteratively for each ω and each x-line wavenumber k_y. This inversion accommodates $v(x)$ variation (lateral variation) naturally through nonstationary $\boldsymbol{U}_{-\Delta z}^A$ and $\boldsymbol{U}_{\Delta z}$. Here $v(x, \Delta z)$, extrapolation depth Δz is split into j small intervals δz_j so that

$$\Delta z = \sum_{j=1}^{n} \delta z_j, \qquad (21)$$

where δz_j is small enough that $\partial_{\delta z_j} v(x, \delta z_j) = 0$. Based on equation 21, then, $\boldsymbol{\psi}_{z+\Delta z}$ is computed recursively as

$$\boldsymbol{\psi}_{z+\Delta z} = \boldsymbol{\psi}_{z+\delta z_1+\delta z_2} = INV_2\left\{INV_1\left\{\boldsymbol{\psi}_z\right\}\right\}, \qquad (22)$$

for example, where INV_2 represents implementation of equation 20 for lateral velocity variation $v(x, \delta z_2)$, and INV_1 accommodates lateral velocity variation $v(x, \delta z_1)$. In general, for Δz divided into n depth steps,

$$\boldsymbol{\psi}_{z+\Delta z} = \boldsymbol{\psi}_{z+\delta z_1+\cdots+\delta z_n} = INV_n\left\{\cdots INV_1\left\{\boldsymbol{\psi}_z\right\}\right\}, \qquad (23)$$

where $\cdots$ indicates recursive application of inversions INV_2 through INV_{n-1}.

When elevation varies, $\boldsymbol{\Delta z} \to \boldsymbol{\Delta z}(\mathbf{x})$, the recursive method of Reshef (1991) is employed. In this method, a zero wavefield is installed at the top of a regular grid where the top of the grid is higher than the highest elevation. Then, based on the near-surface velocity, the zero wavefield is propagated recursively in δz_j intervals until a surface point is reached. If receivers exist there, wavefield data are added at the 'live' locations (Reshef, 1991). Similar to equation 5 in Reshef (1991), modify $\boldsymbol{W_e}$ at each δz_j to give unit weight to 'live' traces, and zero weight to traces elsewhere. Recursive inversion is then computed according to equation 23 until a datum is reached.

EXAMPLES

Two examples demonstrate regularization and WE statics by the inversion method presented here. The first example consists of two synthetic data sets that exhibit aliasing. The first synthetic consists of a superposition of point sources and a line source in a medium whose velocity varies linearly, and where the recording surface has significant elevation change. Linear variation plays to the strength of the inversion in that convergence depends (partially) on spatial derivatives of velocity (as in equation 12), and is presented as the *best case* of a heterogeneous medium. The second synthetic has the same geometry as the linear example, but its step variation in velocity is presented as a challenge to the inversion method. Again, because convergence of the inversion depends on spatial derivatives, step variation will reveal effects due to non-convergence. Aliasing in all examples is achieved through random decimation of traces.

A real data example based on the Husky dataset (Stork, 1994) is then presented. A common source-gather from this dataset is severely decimated based on a common receiver-gather that is very sparse and irregular. The required velocity model of the near-surface is obtained through turning-wave tomography.

Synthetic data examples

Finite differences are used to generate synthetic data based on the velocity models and source / receiver geometries of Figures 1a and b. These data are then decimated in two stages of increasing severity and inversion is performed. Inversion is then followed by phase-shift redatuming to the highest receiver elevation with the mean of the velocity model as a reference velocity. Here, the mean velocity is used to reduce both evanescent leakage and dip-limiting of diffraction tails.

Linear velocity variation

Data that correspond to the linear model in Figure 1a are given in Figure 2a. Here, the original gather is decimated randomly from 512 traces to 256. Inversion of these data based on the velocity model of Figure 1a regularizes the traces and applies WE statics, and the result is given in Figure 2b. Time variation due to elevation and velocity changes is removed, and the event associated with the line source is now linear and continuous. Diffractions associated with the point sources are reconstructed and continuous to high dip. Aliased energy, as indicated in Figure 2c is now removed as can be seen in Figure 2d.

For comparison, the original gather is decimated *evenly* (as opposed to randomly) from 512 to 256 traces (Figure 3a), and interpolation by the $f - x$ method of Spitz (1991) followed by WE statics is performed. Note, null traces used as place holders in Figure 3a are removed prior to $f - x$ interpolation. Though the styles of decimation are quite different (random vs. even), $f - x$ interpolation (aliased, even sampling) and regularization by inversion (aliased, random sampling) are quite similar. Both approaches result in continuous linear events and diffractions, and aliasing is eliminated.

The original gather is then decimated randomly to one third of the original number

of traces ($512 \rightarrow 171$, Figure 4a), and inversion is performed again. Though aliasing is now more severe (Figure 4c), inversion returns continuous events (4b) and an unaliased spectrum (Figure 4d).

Step velocity variation

As a challenge to the inversion presented here, a trace gather based on the step model of Figure 1b is generated, and then decimated randomly from 512 traces to 256 traces (Figure 5a). Though a large, discontinuous change in velocity (2000 m/s $\rightarrow$ 3725 m/s at 2.5 km in Figure 1b) is present in this model, convergence of the inversion is sufficient such that a good result is returned. As can be seen in Figure 5b, events are continuous though artifacts (discussed in the next paragraph) are present at ~ 0.3 seconds between ~ 3000 m and ~ 4200 m. Aliased energy (Figure 5c), as before, is now removed (Figure 5d).

Similar to the linear example, the original gather is decimated evenly ($512 \rightarrow 256$ traces, Figure 6a), and $f - x$ interpolation and WE statics are performed. Again, though we compare random vs. even decimation, regularization of the randomly sampled gather by inversion is comparable to $f - x$ interpolation of the regular gather. Artifacts apparent on the regularized gather (~ 0.3 seconds between ~ 3000 m and ~ 4200 m, Figure 5b) are present, to a slightly lesser extent, on the interpolated gather (Figure 6b). These artifacts are due, presumably, to some shared aspect of these two very different algorithms. Commonalities might include wave-equation operators central to both WE statics (here applied following $f - x$ interpolation) and inversion, or perhaps due to the finite-difference algorithm employed to generate the input data. Regardless, the similarity of regularization and interpolation under these extreme conditions lends confidence to the inversion method.

The original gather is then decimated randomly to one third of the original number of traces ($512 \rightarrow 171$, Figure 7a), and inversion is performed. Though aliasing is now more severe (Figure 7c), inversion returns continuous events (Figure 7b) and an unaliased spectrum (Figure 7d).

Real data example

Figure 8 is a common-source gather obtained form the Husky dataset (Stork, 1994). The elevation profile indicates 300 m of elevation change, and the corresponding spectrum (Figure 8b) shows that data are not aliased. Five reflectors numbered 1 through 5 are indicated on Figure 8a. Of these, arrows associated with reflectors 2 through 5 point to distance 13 000 m – the distance associated with the datum level (lowest elevation). WE statics will not time shift these reflectors at this distance, so they are indicated here and on all subsequent examples as points from which direct comparison between input and output is made. The marker for reflector 1 is offset from the others because, though it is a strong event, it does not persist laterally to distance 13 000 m.

Velocity variation in the near surface is significant for this gather as can be seen in Figure 9. This velocity model is obtained by turning-wave tomography, and it is based on first breaks picked on the entire data volume. Velocity variation is strong in the vertical and horizontal dimensions with a minimum velocity of 2900 m/s at the surface and a maximum

velocity of 4200 m/s at 300 m elevation. The combined effects of topographic and velocity variation result in *push up* and *pull down* of reflections as is apparent, for example, in Figure 8a – a flipped pattern of the topography is imprinted on all reflectors.

Though in the synthetic examples, interpolation of aliased, regularly sampled data, and regularization of aliased, irregularly sample data return similar results, real data often presents unforeseen challenges. So, to verify inversion, the common-source gather of Figure 8 is decimated evenly to half the number of original traces ($306 \rightarrow 153$ traces, Figure 10a) so that an aliased spectrum results (Figure 10b). These data are then interpolated by both inversion and by the $f - x$ method of Spitz (1991) where $f - x$ is followed by WE statics. The $f - x$ result is given in Figure 11. Here, continuity of reflectors is preserved, and lateral coherence of these events is enhanced when reflection events 1 through 5 are compared to those on Figure 8a. The spectrum in Figure 11b shows successful de-aliasing when compared to the aliased spectrum in Figure 10b.

The inversion result given in Figure 12 is comparable directly to the $f - x$ result (Figure 11) in terms of reflector continuity. A small amount of ground-roll leakage is apparent beginning at about 0.5 s to the left of the source location, and it is found to be the result of the use of the chosen value for ε ($\varepsilon = 0.3$). When $\varepsilon = 1$, for example, ground roll is mostly eliminated, but reflectors have a *wormy* appearance. Values of $\varepsilon < 0.3$ result in undesirable growth of amplitude. As shown in Figure 12 b, the data are now de-aliased. Note, during inversion, topographic variation is accommodated according to the adaption of Reshef (1991) that is described in the *Implementation* section above. That is, $\boldsymbol{W_e}$ (implicit in equation 22) is modified at each δz_j to give unit weight to 'live' traces, and zero weight to traces elsewhere. Actual missing traces are always given zero-weight, and zero-weight is given to those traces lower than the depth associated with the current recursion.

The common-source gather is then decimated from the original 306 traces to 60 traces or about 20% of the original number of traces. The 60 live trace locations coincide with those from a common-receiver gather at the same location. Trace spacing is pseudo-random. As Figure 13a shows, large trace gaps are present (for example between 750 m and 900 m distance), and the lateral extent of all reflectors, with the exception of reflector 5, is ambiguous due to severe aliasing. Severe aliasing is verified in the spectrum of Figure 13b. Inversion of the data of figure 13a is given in Figure 14. Though based only on 60 traces, this regularization result is comparable to the 256 trace interpolations of Figures 11 and 12. A significant difference is found on reflector 1 – it lacks coherence laterally beyond 10 100 m to the left from the marker. Reflection events 2 through 5 are well constructed as can be seen on Figure 13a, and much of the aliasing is eliminated. Aliasing does, however, appear to be present above 50 Hz between wavenumbers -0.01 m^{-1} and 0 m^{-1}. Here, a value of 0.5 is used for ε is used to ensure stability at the expense of some smoothness in appearance.

DISCUSSION

Though the development of Ferguson (2006) results in improvements in computational efficiency, diagonal limiting provides little analytic insight, for example for error analysis, or for development of further improvements, so the analytic approximation to S pre-

sented here is desirable. The current work provides not only a functioning inversion, it also provides an analytic framework by which accuracy and computational cost may be analyzed with precision. Experimentally, it is found that, as random trace decimation increases significantly beyond one third, inversion begins to fail beginning with the largest wavenumbers and highest frequencies within the evanescent region. So, given the analytic framework provided here, an exact analysis of error associated with trace decimation is possible – the approximate and exact operators need only be compared for the highest frequency and largest wavenumber of interest. Then, based on a maximum-allowable error for this frequency / wavenumber combination, a minimum number of terms in the approximate operator can be deduced with the assurance that error decreases with frequency and wavenumber.

Adapted for an an entire survey, a few gathers spread across the entire aperture could be procured, and a space dependent value for ε could be constructed. Besides space variable ε, there might be great advantage in the implementation of energy-adaptive stabilization of Duijndam et al. (1999) whereby ε becomes ω and z dependent as well.

Though not explored here, the approximation for S is expected to be suitable as a preconditioning operator for gradient methods. Recently, WE regularization and redatum is implemented as a gradient method (Smith et al., 2009), however, only identity I is used there as a preconditioner. The use of at least one higher-order term of S given in this paper could drastically improve the rate of convergence and the quality of the solution.

CONCLUSIONS

In this paper, the problem of statics and irregular acquisition geometry are addressed simultaneously by least squares. Statics are accommodated in this inversion by the use of one-way wave operators, and irregular sampling in space is accommodated using weighting operators. A minimum smoothness criterion is used to ensure that a unique solution is determined. Efficiency is assured through the use of series expansion of the Hessian. Series expansion reduces the number of Fourier integrals from six to two, and under the 2D assumption, the number of integrals is reduced from three to one. Computationally, it is shown that proportional cost is reduced from N^8 to $m\,N^2$, where N is number of traces in the inline and crossline directions, and n is a small scalar, $n = 4$ for example. Assuming 2D, proportional cost is reduced from N^3 to $n\,N$.

Real and synthetic examples are used to demonstrate the inversion. Synthetic data show that inversion of irregular, aliased data and $f - x$ interpolation of regular, aliased data return equivalent results for the same number of traces. Significant topography and velocity variation is present in the synthetic data so, for direct comparison, wave equation statics (WE) are applied after $f - x$ interpolation. The synthetic data are decimated randomly to one third the number of original traces, and the inversion result is found to be regularized, redatumed, and anti-aliased.

Similar tests performed with real data show that, for regular, aliased data, inversion and $f - x$ interpolation return similar, anti-aliased results. When the real data are decimated randomly to one fifth the number of traces, inversion still returns regularized data that are
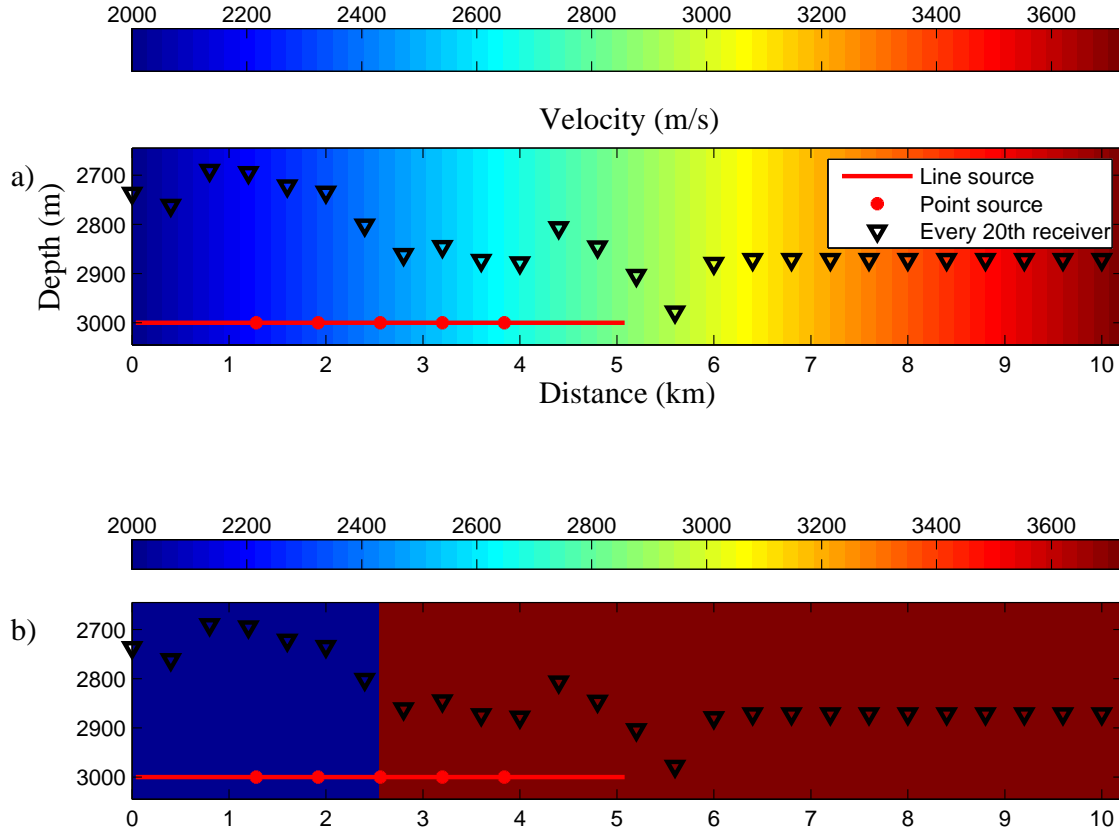
FIG. 1. Velocity models with source/receiver geometry annotated. a) Linear velocity variation. b) A step-function velocity.

redatumed and anti-aliased.

COMPUTATIONAL COST IN 3D

Operator S (equation 4) is a nonstationary integral (Margrave, 1998) over six coordinates $k_x \to (k_{x_1}, k_{x_2})$, $y \to (y_1, y_2)$, and $k'_x \to (k'_{x_1}, k'_{x_2})$. Because common inversion algorithms are based on matrices, computational cost for S may be contemplated according to how many floating-point operations (flops) are required to produce matrix $S(\hat{x}, \hat{x} - x')$ for one output location $\hat{x}$. That is, operator S maps the entire, arbitrary wavefield ψ_z to a single output location $\hat{x}$ according to

$$[S\psi_z(x')](\hat{x}) = \int \psi_z(x') S(\hat{x}, \hat{x} - x') \, dx'. \tag{24}$$
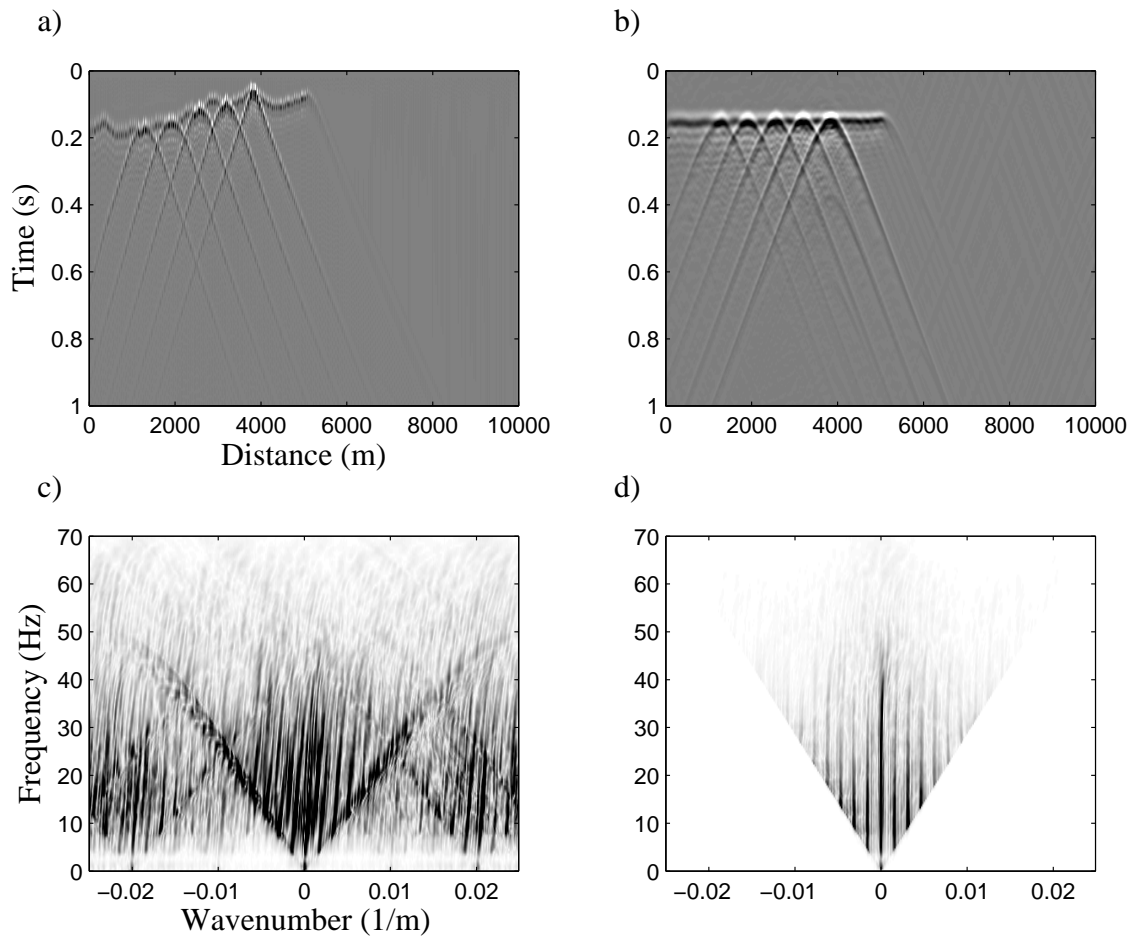
FIG. 2. Irregularly sampled synthetic data corresponding to the linear model of Figure 1a. a) Aliased data (256 traces spaced randomly). b) Regularization and WE statics by inversion. c) Spectrum of a). d) Spectrum of b).
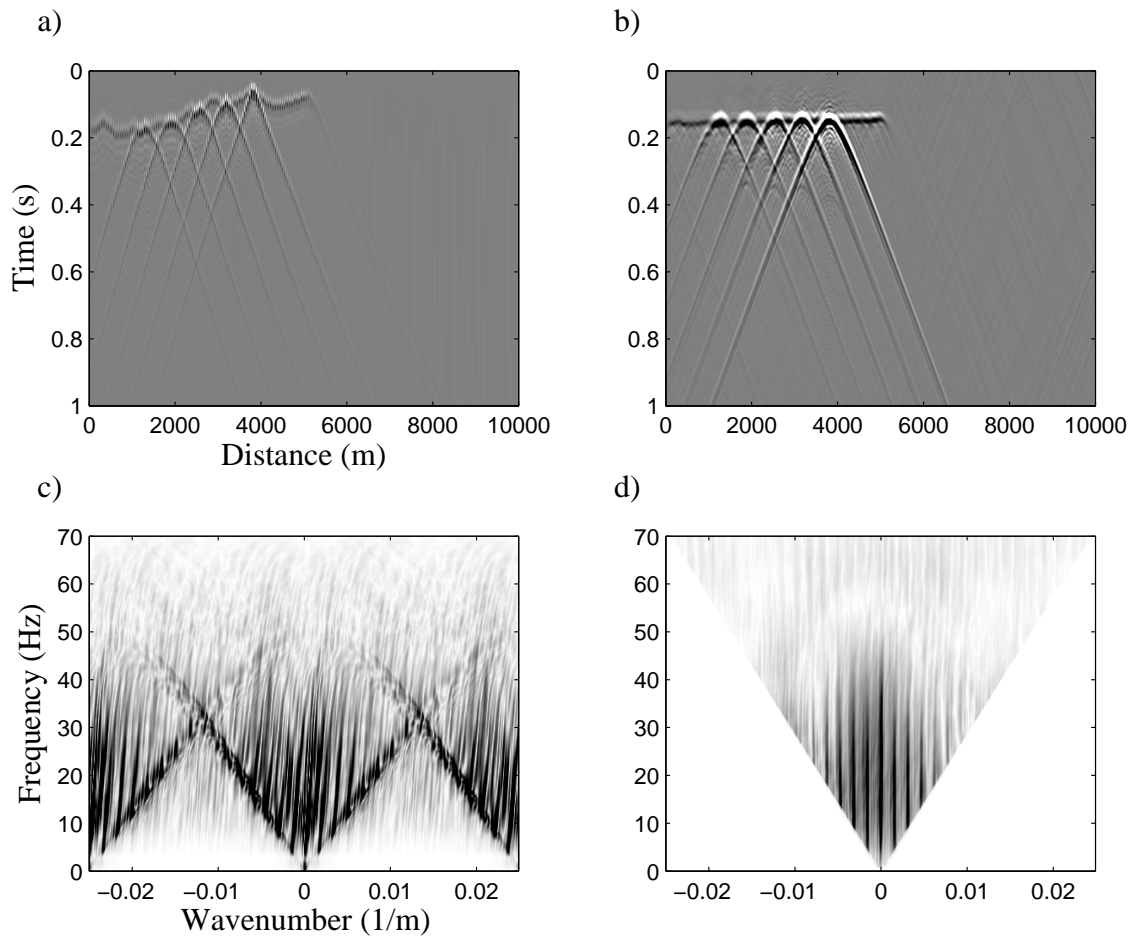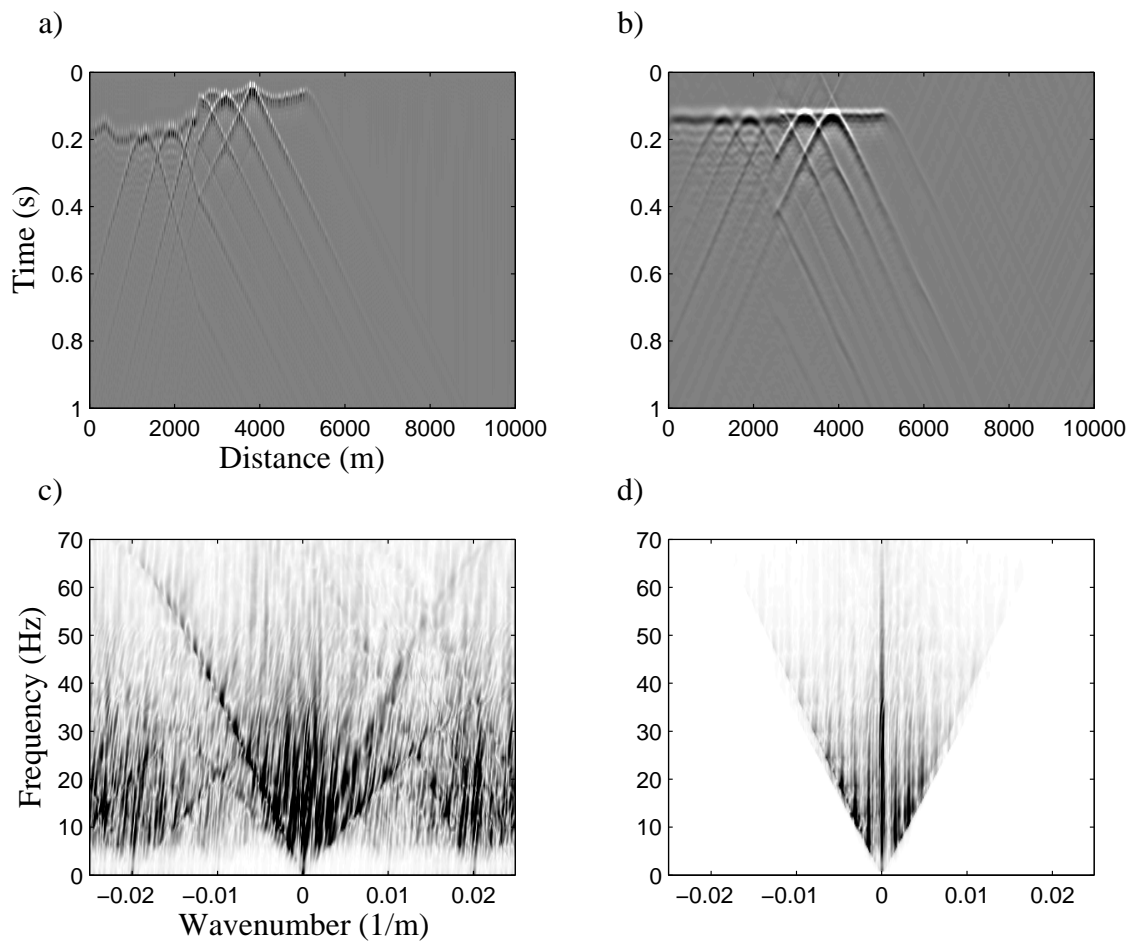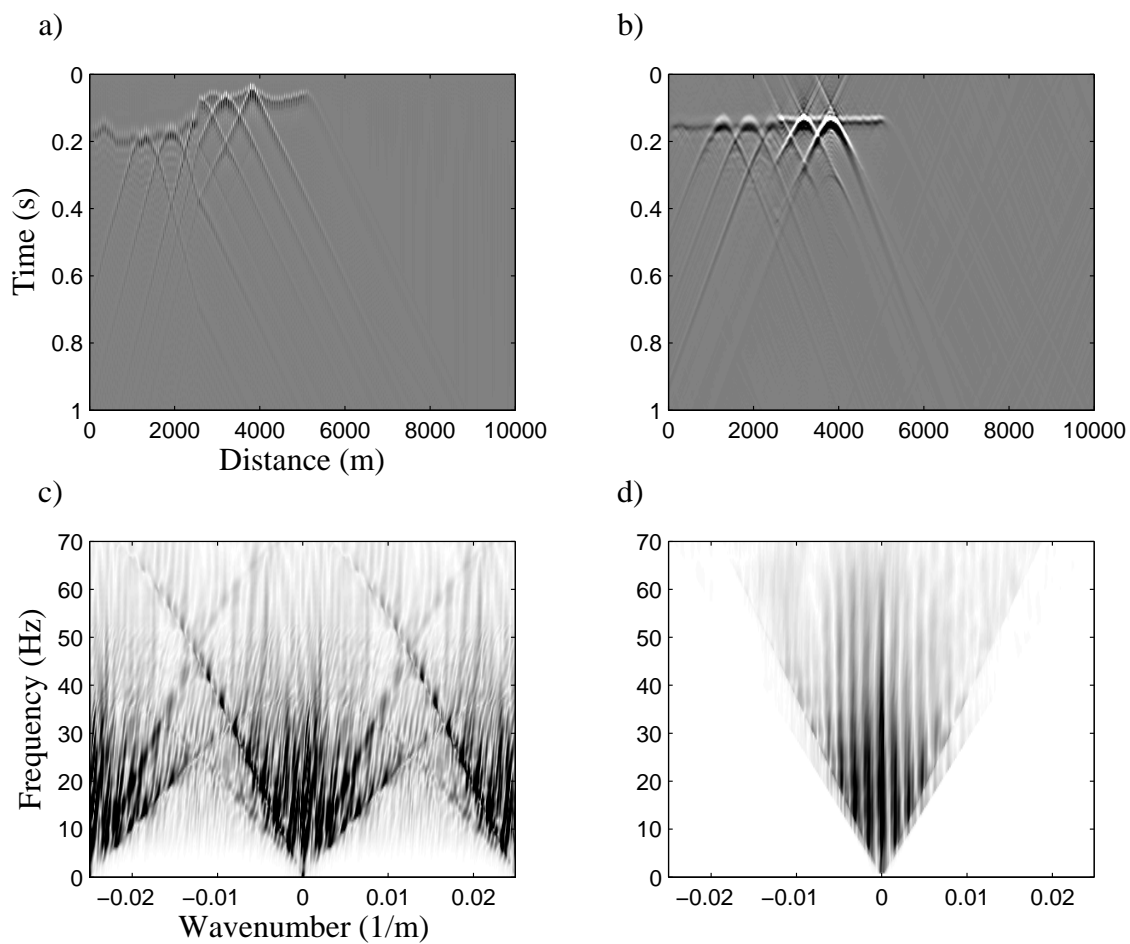
FIG. 3. Regularly sampled (in space), but aliased, synthetic data corresponding to the linear model of Figure 1a. a) Aliased data (256 traces spaced evenly). b) Interpolation by the $f - x$ method of Spitz (1991) followed by WE statics. c) Spectrum of a). d) Spectrum of b).
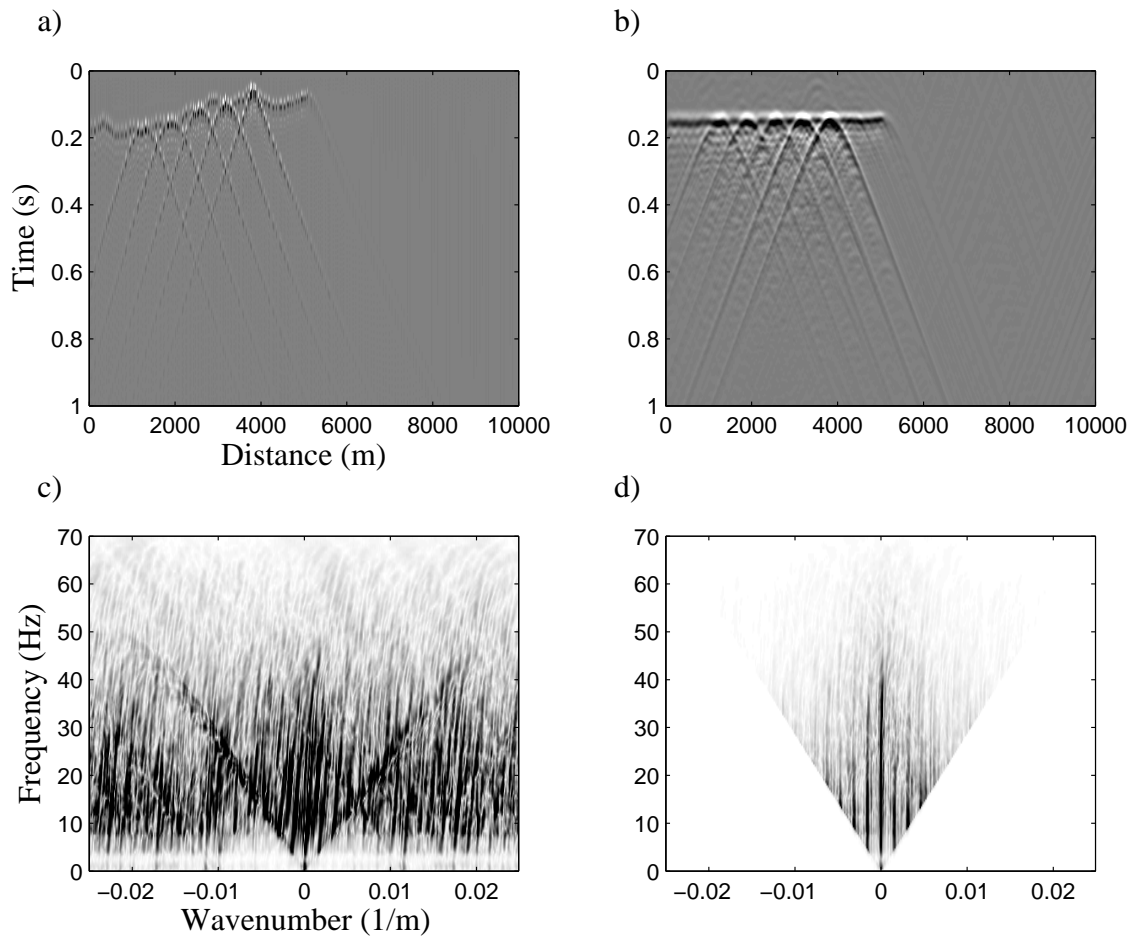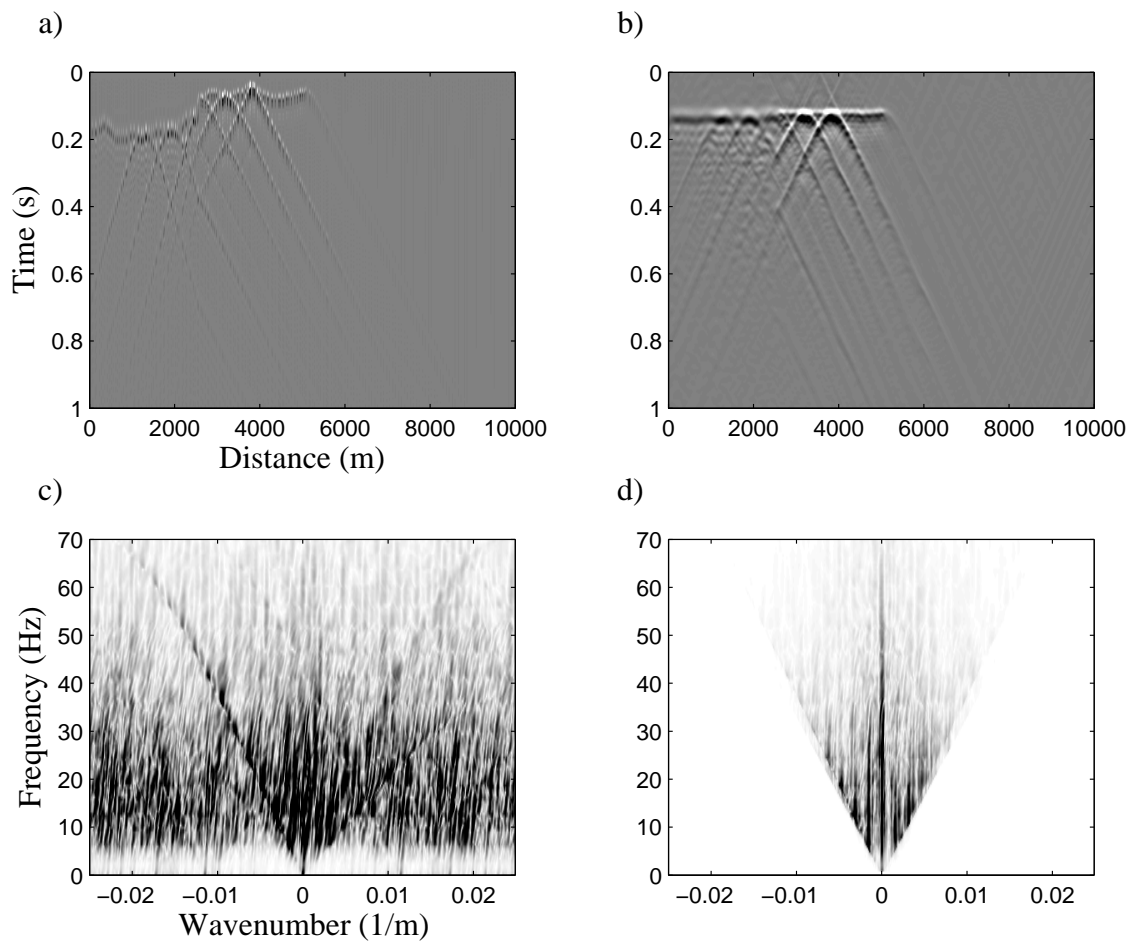
FIG. 4. Irregularly sampled synthetic data corresponding to the linear model of Figure 1a. a) Aliased data (171 traces spaced randomly). b) Regularization and WE statics by inversion. c) Spectrum of a). d) Spectrum of b).

a)

b)

c)

d)

FIG. 5. Irregularly sampled synthetic data corresponding to the step model of Figure 1b. a) Aliased data (256 traces spaced randomly). b) Regularization and WE statics by inversion. c) Spectrum of a). d) Spectrum of b).

FIG. 6. Regularly sampled, but aliased, synthetic data corresponding to the step model of Figure 1b. a) Aliased data (256 traces spaced evenly). b) Interpolation by the $f - x$ method of Spitz (1991) followed by WE statics. c) Spectrum of a). d) Spectrum of b).

FIG. 7. Irregularly sampled synthetic data corresponding to the step model of Figure 1b. a) Aliased data (171 traces spaced randomly). b) Regularization and WE statics by inversion. c) Spectrum of a). d) Spectrum of b).
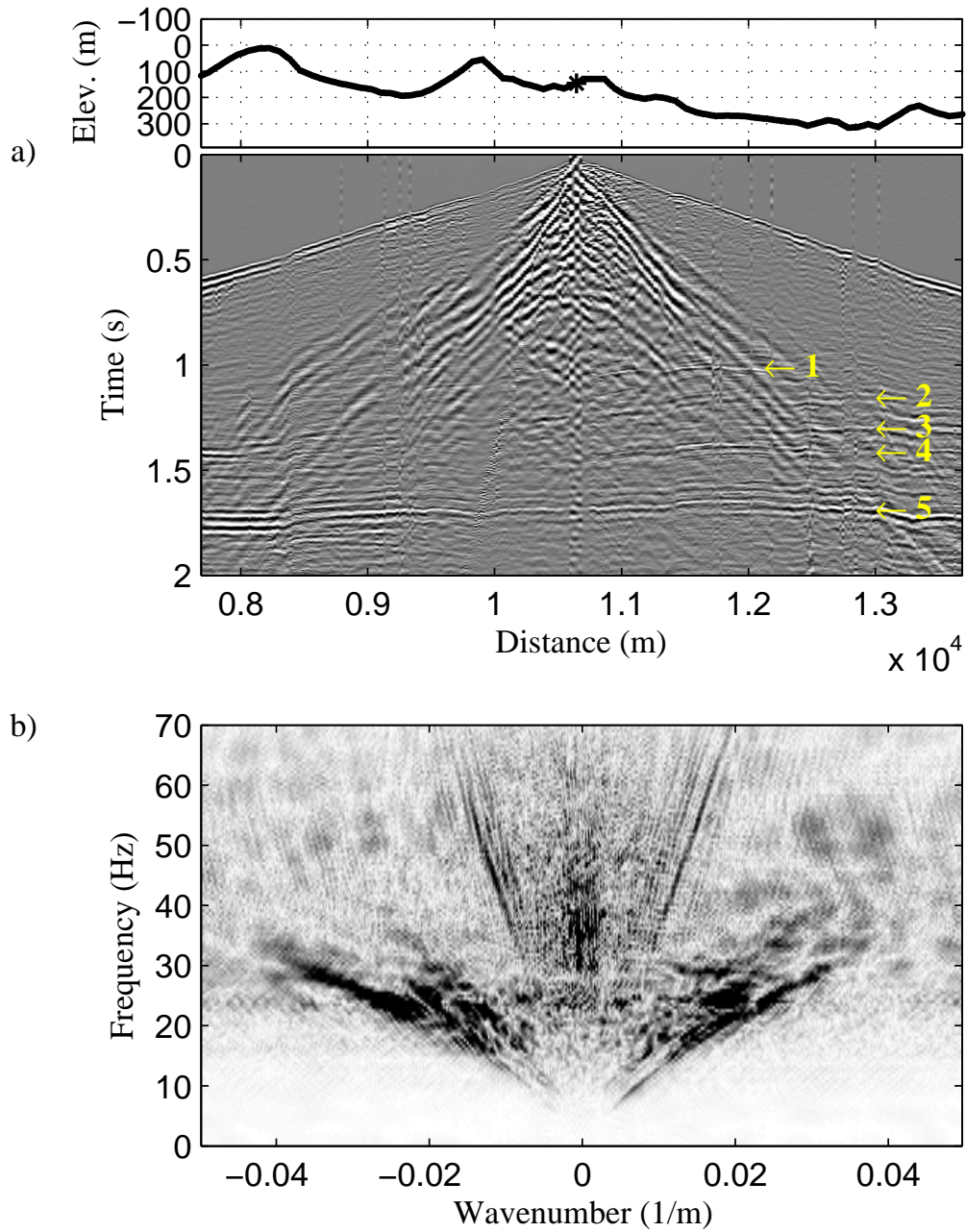
FIG. 8. Common shot gather from the Husky dataset (Stork, 1994). a) Seismic data (306 traces evenly spaced) plus an elevation profile. Triangles indicate coherent reflections. b) Spectrum of a).
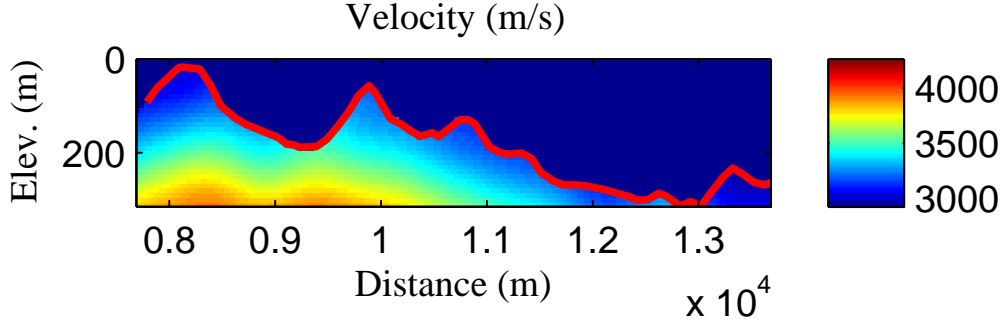
FIG. 9. Velocity model of the near surface derived from turning-wave tomography. Surface topography is indicated by the red line. Velocity varies between 2900 m/s (dark blue) to 4200 m/s (red).

Inversion by equation 1, then, proceeds one output-location at a time according to

$$\psi_{z+\Delta z}\left(\hat{x}\right) = \int \left[S\left(\hat{x}, \hat{x} - x'\right) + \varepsilon^2 W_m\right]^{-1} U^A_{-\Delta z}\left(\hat{x}, \hat{x} - x'\right) W_e\left(x'\right) \psi_z\left(x'\right) \, dx', \quad (25)$$

where integration over x' is written here explicitly, and extrapolator $U^A_{-\Delta z}$ is parametrized to map wavefield ψ_z to $\hat{x}$. To estimate cost for fixed output location $\hat{x}$, S (equation 4) as an $N \times N$ matrix operator is

$$S\left(\hat{x}, \hat{x} - x'\right) = \frac{1}{(2\pi)^2} \int A\left(k_x, k'_x\right) e^{i\,[k_x, x']} e^{-i\,[k'_x, \hat{x}]} dk_x \, dk'_x, \quad (26)$$

where x', k_x and k'_x each have dimension $N \times N$, and

$$A\left(k_x, k'_x\right) = \frac{1}{(2\pi)^2} \int e^{-i\,[k_x, y]} e^{i\,[k'_x, y]} \alpha\left(y, k'_x\right)_{\Delta z} \tilde{\alpha}\left(y, k'_x\right)_{-\Delta z} \, dy. \quad (27)$$

Here, we assume that the irregular input array of dimension $m \times n$, where m and n are not necessarily equal, is padded with null traces to dimension $N \times N$ where $m \le N$ and / or $n \le N$ (i.e., x' has dimension $N \times N$).

For fixed wavenumbers $\hat{k}_x$ and $\hat{k}'_x$, A (equation 27) is a two-dimensional integral with cost $\propto N^2$ flops. Computationally, then, $A\left(\hat{k}_x, \hat{k}'_x\right)$ resides within the inner-loop of an iterative, 2D inversion. To consider total cost, keep $k_x = \hat{k}_x$ fixed, and compute matrix $A\left(\hat{k}_x, k'_x\right)$ for all k'_x - cost is $\propto N^2 \times$ the cost of each $A\left(\hat{k}_x, \hat{k}'_x\right)$, or $\propto N^2 \times N^2 = N^4$. Next, according to equation 26, multiply matrix $A\left(\hat{k}_x, \hat{k}'_x\right)$ by $\frac{1}{(2\pi)^2} e^{-i\,[k'_x, \hat{x}]}$, and then sum over k'_x. Cost for this multiplication and then sum is $\propto N^2$ and can be neglected when only the highest order cost N^4 is considered. Repeat this process N^2 times for each k_x, multiply by $e^{i\,[\hat{k}_x, x']}$ and sum into S (according to equation 26) at each iteration. This cost, then, is $\propto N^2 \times N^4 = N^6$ flops. Recall, however, that only a single output location $\hat{x}$ has been produced. To compute the entire monochromatic wavefield $\psi\left(x\right)$, the process above must be repeated N^2 times for a minimum total cost $\propto N^2 \times N^6 = N^8$.
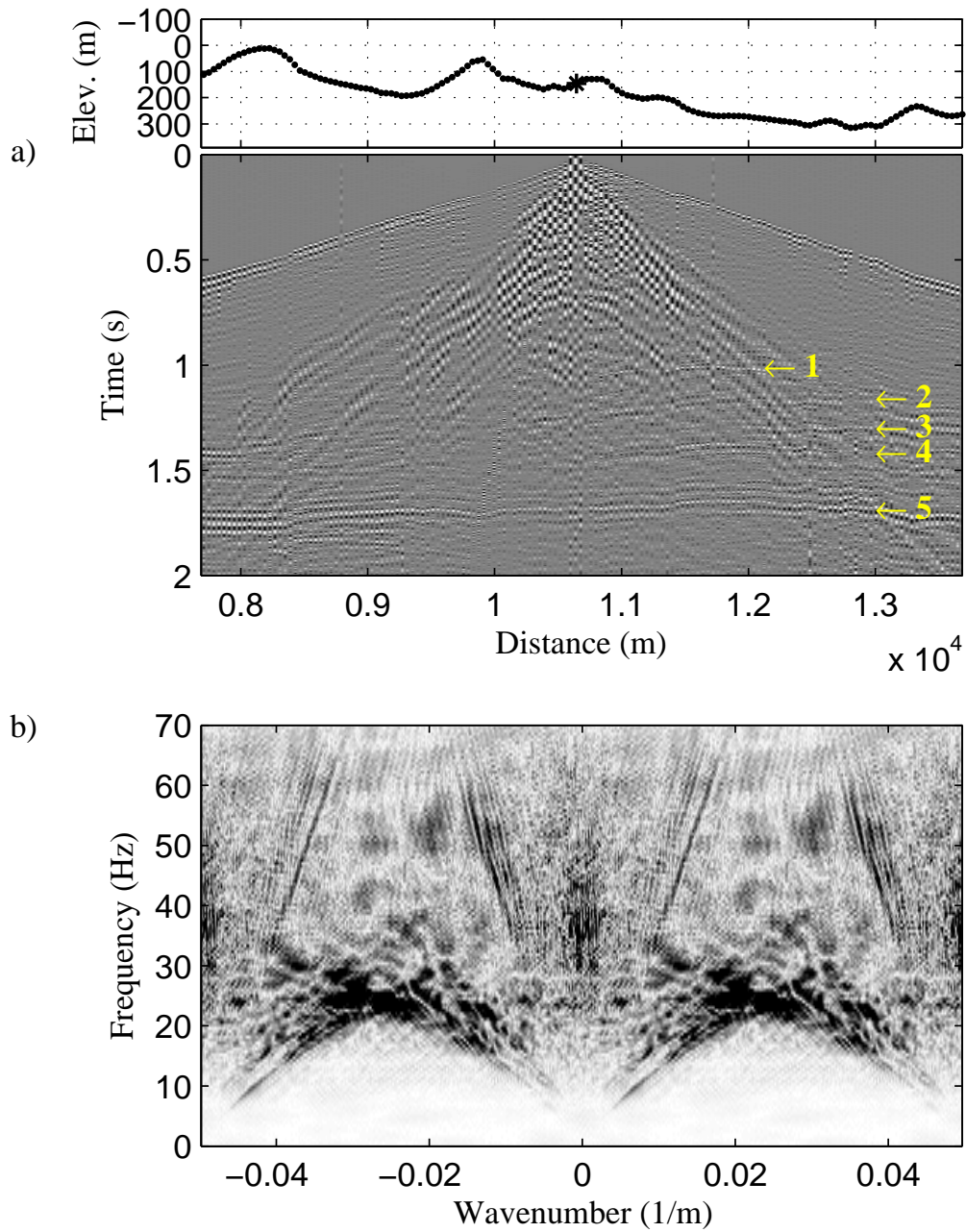
FIG. 10. Regularly sampled, but aliased, shot gather. a) Seismic data (145 / 306 traces evenly spaced) plus an elevation profile. b) Spectrum of a).
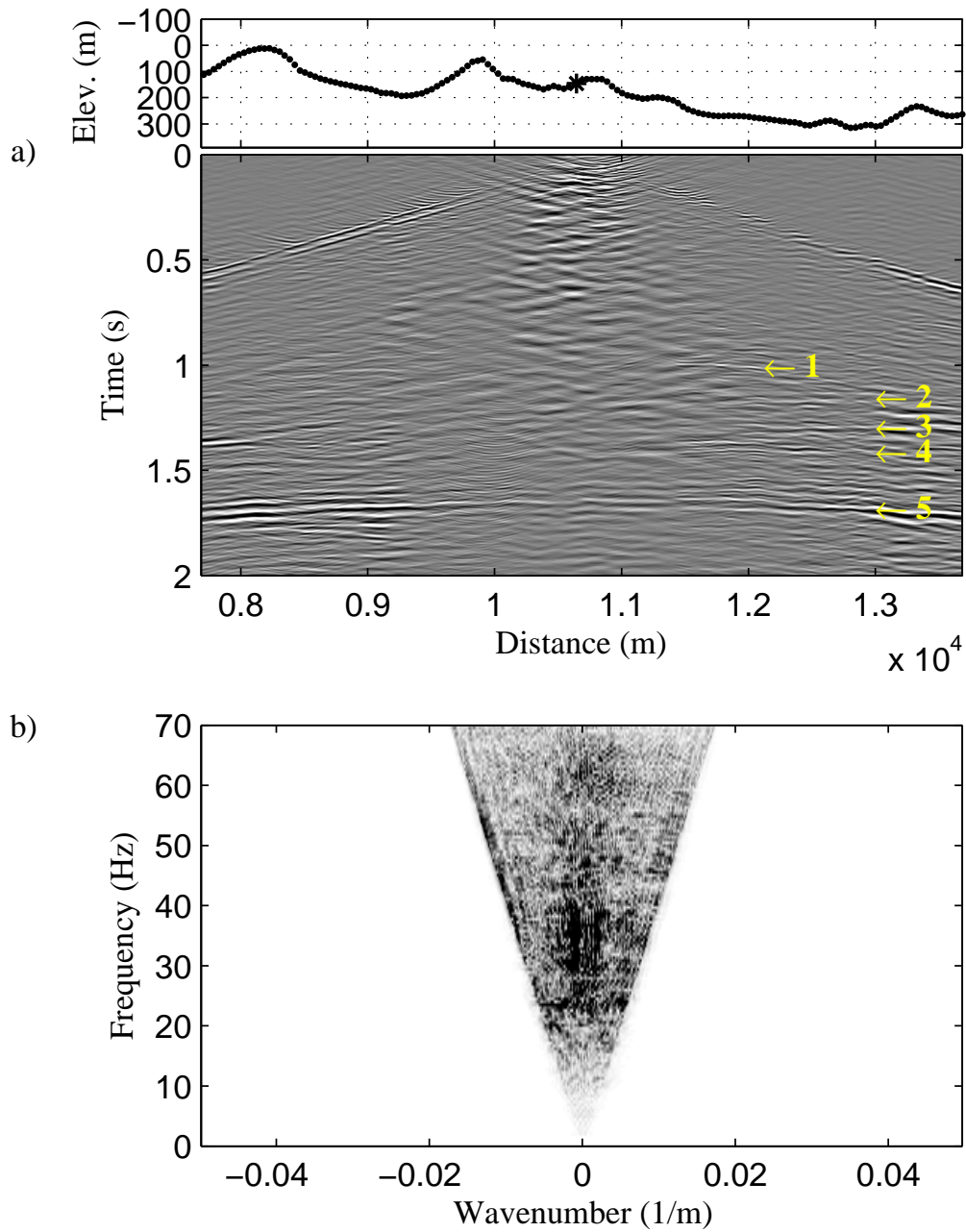
FIG. 11. Interpolation of Figure 10 by the $f - x$ method of Spitz (1991) followed by WE statics. a) Interpolated data. b) Spectrum of a).
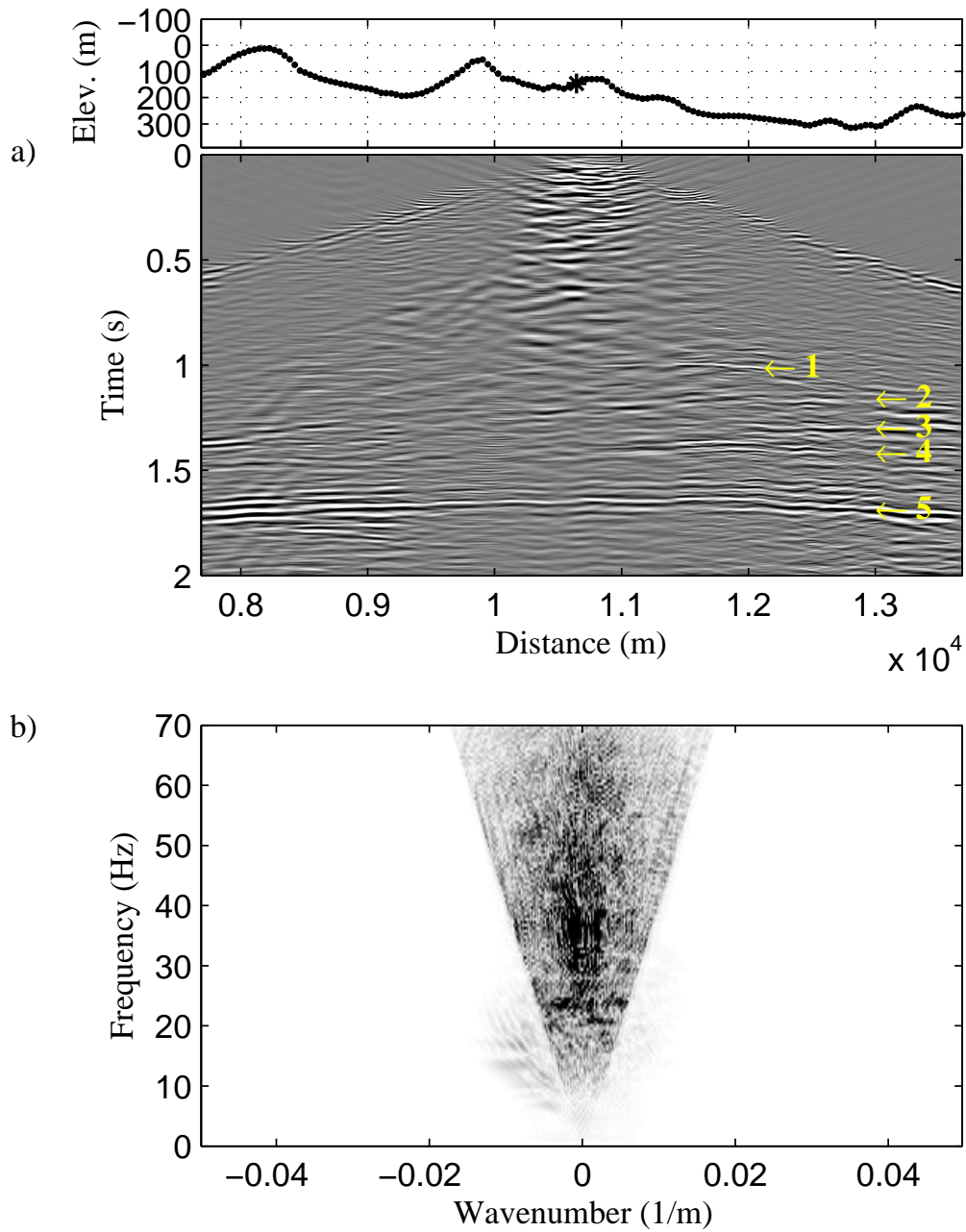
FIG. 12. Interpolation of Figure 10 and WE statics by inversion. a) Interpolated data. b) Spectrum of a).
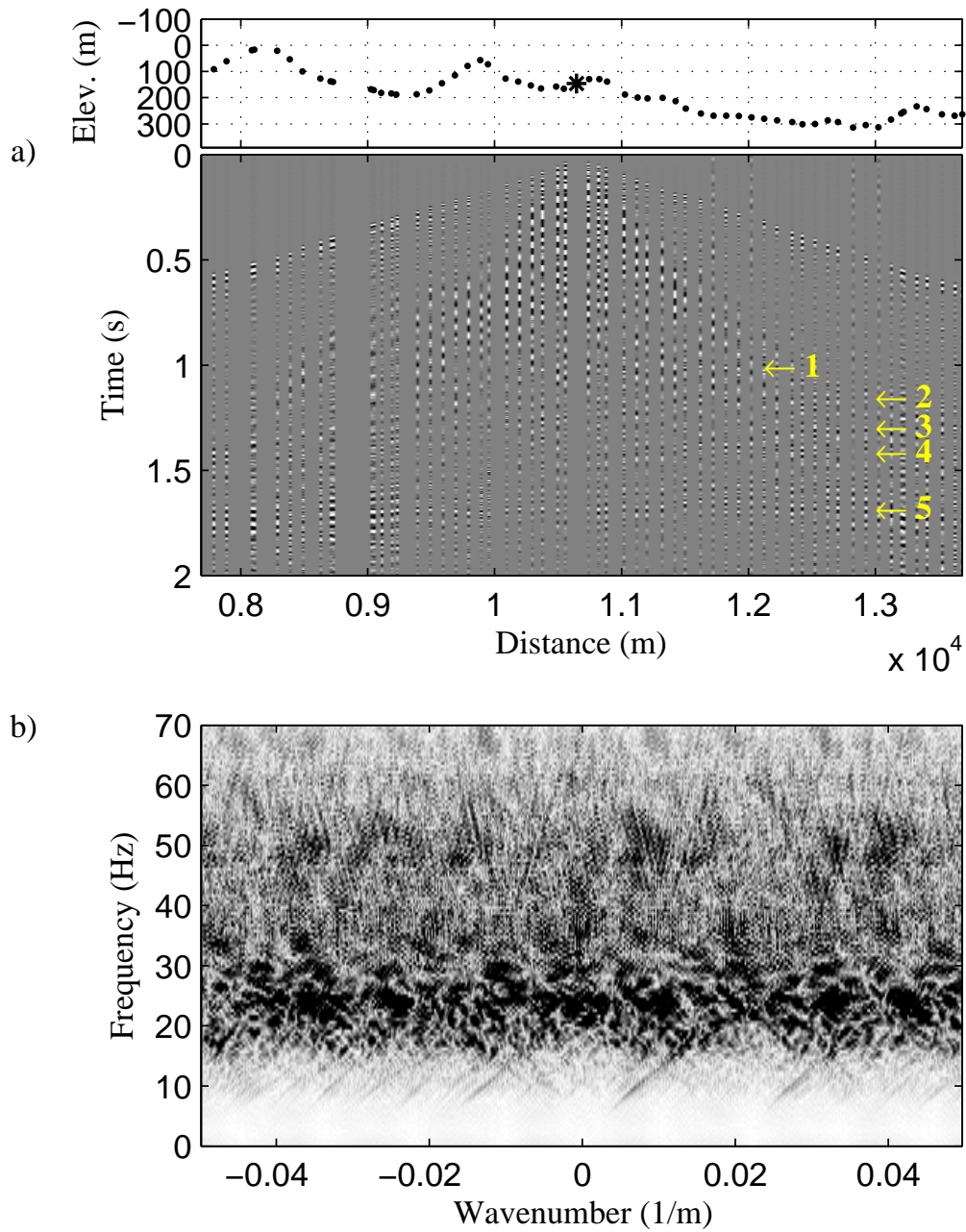
FIG. 13. Irregularly sampled shot gather from the Husky dataset (Stork, 1994). a) Seismic data (60 / 306 traces randomly spaced) plus an elevation profile. b) Spectrum of a).
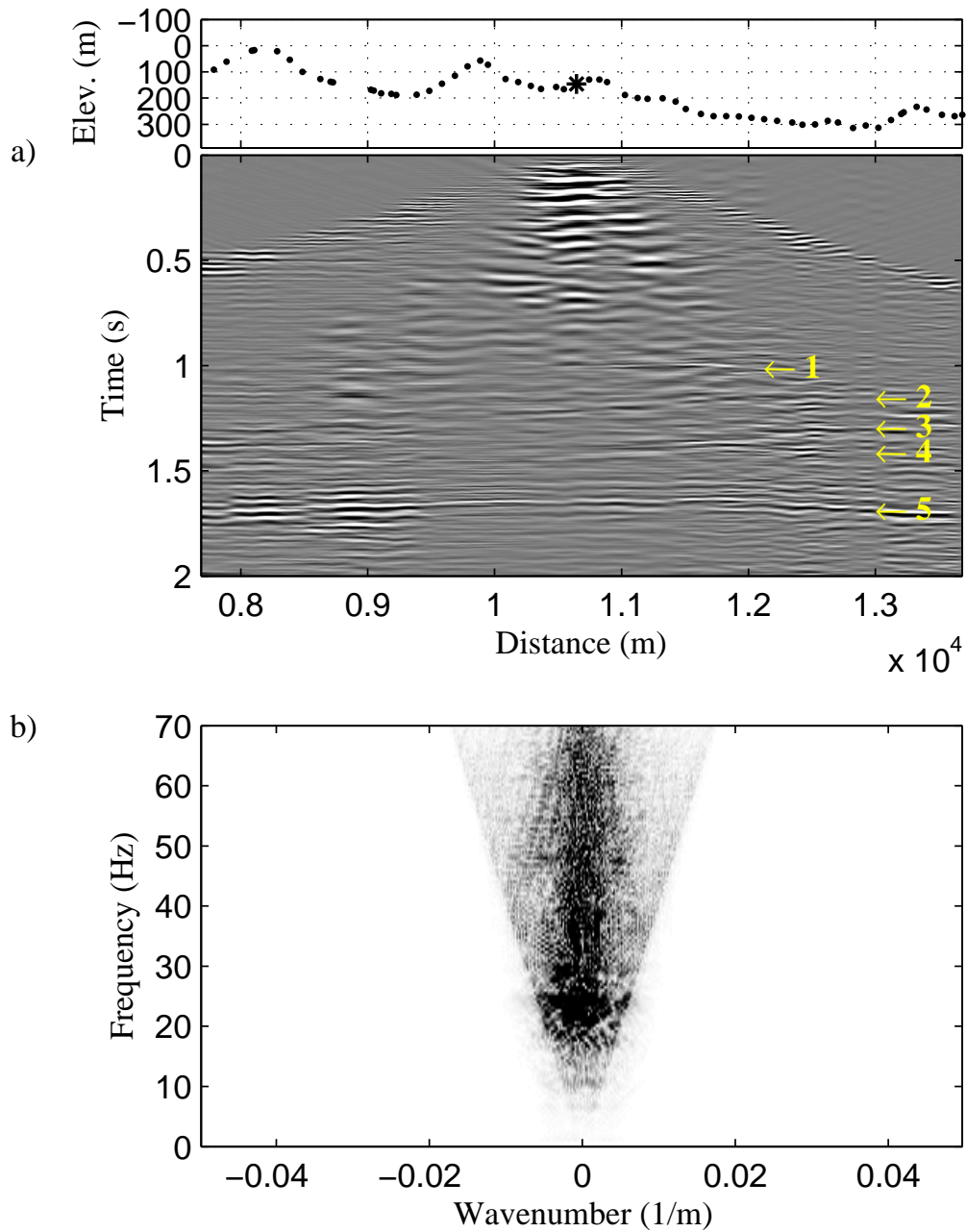
FIG. 14. Regularization of Figure 13 and WE statics by inversion. a) Regularized data.

REFERENCES

Abma, R., and Kabir, N., 2006, 3D interpolation of irregular data with a POCS algorithm: Geophysics, **71**, No. 6, E91–E97.
URL http://link.aip.org/link/?GPY/71/E91/1

Berkhout, A. J., 1985, Seismic Migration. Imaging of acoustic energy by wavefield extrapolation. A. Theoretical aspects: Elsevier.

Duijndam, A. J. W., and Schonewille, M. A., 1999, Nonuniform fast Fourier transform: Geophysics, **64**, No. 2, 539–551.

Duijndam, A. J. W., Schonewille, M. A., and Hindriks, C. O. H., 1999, Reconstruction of band-limited signals, irregularly sampled along one spatial direction: Geophysics, **64**, No. 2, 524–538.

Etgen, J. T. E., 1994, Stability of explicit depth extrapolation through laterally varying media, *in* 64th Ann. Internat. Mtg, Soc. of Expl. Geophys., 1266–1269.

Ferguson, R. J., 2006, Regularization and datuming of seismic data by weighted, damped least-squares: Geophysics, **71**, No. 5, U67 – U76.

Gazdag, J., and Sguazzero, P., 1984, Migration of seismic data by phase-shift plus interpolation: Geophysics, **49**, No. 02, 124–131.

Güliünay, N., 2003, Seismic trace interpolation in the Fourier transform domain: Geophysics, **68**, No. 1, 355–369.

Hennenfent, G., and Herrmann, F. J., 2008, Simply denoise: Wavefield reconstruction via jittered undersampling: Geophysics, **73**, No. 3, V19–V28.
URL http://link.aip.org/link/?GPYSA7/73/V19/1

Hu, J., Schuster, G. T., and Valasek, P., 2001, Poststack migration deconvolution: Geophysics, **66**, No. 3, 939–952.

Kühl, H., and Sacchi, M. D., 2004, Least-squares wave-equation migration for AVP/AVA inversion: Geophysics, **69**, No. 1, 262–273.

Margrave, G. F., 1998, Theory of nonstationary linear filtering in the Fourier domain with application to time-variant filtering: Geophysics, **63**, No. 01, 244–259.

Margrave, G. F., and Ferguson, R. J., 1999, Wavefield extrapolation by nonstationary phase shift: Geophysics, **64**, No. 4, 1067–1078.

Menke, W., 1989, Geophysical data analysis: Discrete inverse theory: Academic Press.

Naghizadeh, M., and Sacchi, M. D., 2009, $f - x$ adaptive seismic-trace interpolation: Geophysics, **74**, No. 1, V9–V16.
URL http://link.aip.org/link/?GPYSA7/74/V9/1

Press, W. H., Teukolsky, S. A., Vetterling, W. T., and Flannery, B. P., 1999, Numerical recipes in C: Cambridge University Press.

Reshef, M., 1991, Depth migration from irregular surfaces with depth extrapolation methods (short note): Geophysics, **56**, No. 01, 119–122.

Robertsson, J. O. A., Moore, I., Vassallo, M., Azdemir, K., Manen, D. J. V., and Azbek, A., 2008, On the use of multicomponent streamer recordings for reconstruction of pressure wavefields in the crossline direction: Geophysics, **73**, No. 5, A45–A49.
    URL http://link.aip.org/link/?GPYSA7/73/A45/1

Schneider, W. A., 1978, Integral formulation for migration in two-dimensions and three-dimensions: Geophysics, **43**, No. 01, 49–76.

Smith, D. R., Sen, M. K., and Ferguson, R. J., 2009, Regularization and datuming using least squares and conjugate gradients, *in* 71st Mtg., Eur. Assn. Geosci. Eng., V043.

Spitz, S., 1991, Seismic trace interpolation in the $f - x$ domain: Geophysics, **56**, No. 06, 785–794.

Stolt, R. H., 1978, Migration by Fourier transform: Geophysics, **43**, No. 01, 23–48, discussion and reply in GEO-60-5-1583.

Stork, C., 1994, Demonstration of MvA tomography with controls and constraints for determining an accurate velocity model for prestack depth migration, *in* 64th Ann. Internat. Mtg, Soc. of Expl. Geophys., 1338–1342.

Tarantola, A., 1987, Inverse problem theory: Elsevier Science.

Trad, D. O., 2003, Interpolation and multiple attenuation with migration operators: Geophysics, **68**, No. 6, 2043–2054.

Yu, J., Hu, J., Schuster, G. T., and Estill, R., 2006, Prestack migration deconvolution: Geophysics, **71**, No. 2, S53–S62.
    URL http://link.aip.org/link/?GPY/71/S53/1

Zwartjes, P. M., and Sacchi, M. D., 2007, Fourier reconstruction of nonuniformly sampled, aliased seismic data: Geophysics, **72**, No. 1, V21–V32.
    URL http://link.aip.org/link/?GPY/72/V21/1